Mechanics of pH–Responsive Hydrogel Capsules

6 AUTHORS, INCLUDING:

James P Best
Empa - Swiss Federal Laboratories for Materia…
19 PUBLICATIONS **318** CITATIONS

SEE PROFILE

Martin Peter Neubauer
Jungbunzlauer International AG
10 PUBLICATIONS **82** CITATIONS

SEE PROFILE

Henk H Dam
University of Melbourne
17 PUBLICATIONS **517** CITATIONS

SEE PROFILE

Andreas Fery
Leibniz Institute of Polymer Research Dresden
**251** PUBLICATIONS **4,850** CITATIONS

SEE PROFILE

Mechanics of pH-Responsive Hydrogel Capsules

James P. Best,[†] Martin P. Neubauer,[‡] Sameen Javed,[†] Henk H. Dam,[†] Andreas Fery,*[‡] and Frank Caruso*[†]

[†]Department of Chemical and Biomolecular Engineering, The University of Melbourne, Parkville, Victoria 3010, Australia
[‡]Physical Chemistry II, Bayreuth University, 95447 Bayreuth, Germany

S *Supporting Information*

ABSTRACT: While soft hydrogel nano- and microstructures hold great potential for therapeutic treatments and in vivo applications, their nanomechanical characterization remains a challenge. In this paper, soft, single-component, supported hydrogel films were fabricated using pendant-thiol-modified poly(methacrylic acid) (PMA$_{SH}$). The influence of hydrogel architecture on deformation properties was studied by fabricating films on particle supports and producing free-standing capsules. The influence of the degree of thiol-based cross-linking on the mechanical properties of the soft hydrogel systems (core–shell and capsules) was studied using a colloidal-probe (CP) AFM technique. It was found that film mechanical properties, stability, and capsule swelling could be finely tuned by controlling the extent of poly(methacrylic acid) thiol modification. Furthermore, switching the pH from 7.4 to 4.0 led to film densification due to increased hydrogen bonding. Hydrogel capsule systems were found to have stiffness values ranging from 0.9 to 16.9 mN m^{-1} over a thiol modification range of 5 to 20 mol %. These values are significantly greater than those for previously reported PMA$_{SH}$ planar films of 0.7–5.7 mN m^{-1} over the same thiol modification range (Best et al., Soft Matter 2013, 9, 4580–4584). Films on particle substrates had comparable mechanical properties to planar films, demonstrating that while substrate geometry has a negligible effect, membrane and tension effects may play an important role in capsule force resistance. Further, when transitioning from solid-supported films to free-standing capsules, simple predictions of shell stiffness based on modulus changes found for supported films are not valid. Rather, additional effects like diameter increases (geometrical changes) as well as tension buildup need to be taken into account. These results are important for research related to the characterization of soft hydrogel materials and control over their mechanical properties.
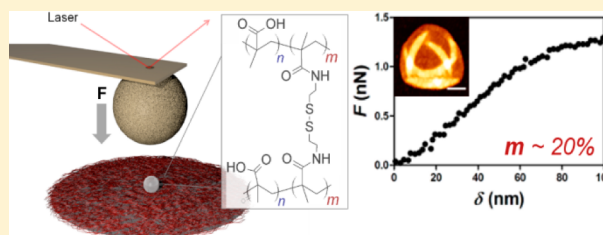
INTRODUCTION

Soft nanostructured planar and particle hydrogel systems are promising for biomedical applications due to their low cytotoxicity and tunable hydration and rigidity.[1–4] Increasingly, research is focusing on the influence of advanced material physicochemical properties on cellular and biological interactions.[5,6] While this is primarily directed to the delivery of therapeutics for in vivo systems, its scope extends as far as the understanding of basic cellular function and activity. In a recent example, Giasson and co-workers investigated the effect of hydrogel nanoparticle uptake by RAW 264.7 murine macrophage cells.[7] The mechanical properties of the hydrogel particles were controlled through the cross-linking degree, and it was found that both the rate and endocytosis mechanism utilized by the cells were governed by the rigidity of the particles studied. In addition to particle systems, the influence of hydrogel film mechanical properties on cellular adhesion, migration, proliferation, and growth has also been studied.[8] We recently reported that by tuning the stiffness of the thiolated hydrogel films presented here, cervical cancer cell adhesion was able to be mediated.[9] Such studies are likely to influence the design of future hydrogel materials for tissue engineering and targeted drug delivery applications. However, our current understanding of the properties of free-standing capsule systems is largely based on studies extrapolated from films assembled on planar supports.

Atomic force microscopy (AFM) force spectroscopy is a useful technique for the mechanical analysis of soft nanostructured materials. AFM has been used for the characterization of planar thin films,[10–12] particles,[7,13] and hollow polyelectrolyte capsules[14–16] with great precision. One of the advantages of such a technique is that single capsules (or particles) can be independently measured, offering considerable mechanical information. However, collecting sufficient data for a reasonable statistical analysis can be time-consuming. Furthering the single particle measurement technique, in 1991 Ducker et al. developed a colloidal probe method for higher sensitivity force measurements.[17] Useful for especially soft materials, a colloidal probe (CP) is attached to the end of a cantilever to increase the interaction area when compared to a sharp tip probe.[18] This also offers the advantage of having a well-defined interaction geometry, tailored surface roughness

and chemistry, and reduced localized axial strain during measurement.[18,19] The latter is particularly important, as for large applied axial strains, material nonlinearity can be observed.[19] The CP-AFM technique has been used for the characterization and Young's modulus (E_Y) determination of polyelectrolyte multilayer films[20] and capsules[21,22] and has been successfully utilized to investigate large hydrogel capsules undergoing pH cycling in buffer under low applied forces.[23] However, apart from the latter study, the tuning and analysis of extremely soft free-standing hydrogel particles has received sparse attention. It is also important to note that while the swelling behavior of planar film and capsule poly(methacrylic acid) (PMA) systems has been investigated,[24,25] no study has compared the mechanical properties of materials on various substrates with different dimensionalities.

Thiol-modified poly(methacrylic acid) (PMA$_{SH}$) can be used to form tunable hydrogel systems that have been the focus of recent studies.[26−28] Single-component films and hydrogel capsules (HCs) can be formed using the layer-by-layer (LbL) assembly technique, through cooperative hydrogen-bonding interactions between PMA and poly(N-vinylpyrrolidone) (PVPON). PMA$_{SH}$ can be then cross-linked through oxidation of the pendant thiol groups into disulfide linkages and the PVPON removed at physiological pH by disrupting the hydrogen bonding network. As the pK_a of PMA is ∼6−7, carboxylic acid groups are deprotonated at pH 7.4, leading to intermolecular charge repulsion and capsule swelling. Cross-linked PMA$_{SH}$ systems, however, are able to form highly hydrated and stable networks at high pH. In addition, the disulfide cross-links between adjacent polymers may be cleaved under reducing conditions, such as for intracellular environments, which may facilitate material degradation and cargo release in vivo. Specifically, PMA$_{SH}$ systems have been shown to be degradable in simulated intracellular conditions[29,30] while demonstrating stability at bloodstream pH.[30] PMA$_{SH}$ capsules can be antibody-functionalized for enhanced cell binding and association[31] and can also encapsulate proteins,[30] oligonucleotides,[32] and double-stranded linear DNA or plasmid DNA.[33] These characteristics demonstrate the considerable promise of PMA$_{SH}$ hydrogel materials for future therapeutic treatments.

In this paper, we quantify the extent of 2-(2-pyridinyldithio)-ethaneamine (PDA) modification of PMA (PMA−PDA), which allows for disulfide cross-link formation, for four different PDA target percentages using UV−vis spectrophotometry. We then examine the structure and LbL assembly of the constituent PMA$_{SH}$ polymers on particle substrates and quantify the mechanical properties. In particular, we investigate how the degree of cross-linking in these systems affects HC film stability and system stiffness, using CP-AFM. This approach allows for the investigation of free-standing shell mechanics in hollow capsule systems, which can then be compared to soft hydrogel planar films previously reported.[9] This provides insights into the effects of hydrogel architecture on mechanical resistances at deformations on the nanoscale.

■ EXPERIMENTAL METHODS

Materials. The pH of all solutions was measured with a Mettler-Toledo MP220 pH meter. High-purity (Milli-Q) water with a resistivity of >18 MΩ cm was obtained from an inline Millipore RiOs/Origin water purification system. Dialysis tubing (68035-35FT) with a MWCO of 3500 Da was obtained from Thermo Scientific. SiO$_2$ particles (1.11 ± 0.05 μm diameter) were purchased from Micro-particles GmbH (Berlin, Germany) as a 50 g L$^{−1}$ suspension.

Poly(methacrylic acid, sodium salt), (PMA-Na, M_W = 15 000 g mol$^{−1}$) was purchased from Polysciences, while PVPON (M_W = 10 000 g mol$^{−1}$), 1-ethyl-3-(3-dimethylaminopropyl)carbodiimide (EDC), dithiothreitol (DTT), polyethyleneimine (PEI, M_W = 25 000 g mol$^{−1}$), phosphate-buffered saline (PBS), 3-(N-morpholino)propanesulfonic acid (MOPS), 2-(N-morpholino)ethanesulfonic acid (MES), sodium acetate (NaOAc), N-chloro-p-toluenesulfonamide sodium salt (CaT), hydrofluoric acid (HF), and PDA were obtained from Sigma-Aldrich. All chemicals were used as received. Mica (grade V-4) substrates of 22 mm diameter were sourced from SPI Chem. PMA−PDA was synthesized and characterized using nuclear magnetic resonance spectroscopy (^{1}H NMR, 500 MHz Varian INOVA system at 25 °C) as previously reported.[9]

Prior to LbL assembly, the PMA−PDA precursor was reduced to PMA$_{SH}$ through cleavage of the PDA group. The reduction required a 0.5 M DTT solution in 50 mM MOPS buffer (pH 8) for 30 min at 37 °C with constant agitation. The resultant PMA$_{SH}$ solution was then diluted with 100 mM NaOAc buffer (pH 4) to 0.5 mg mL$^{−1}$ for planar films or 2 mg mL$^{−1}$ for HC LbL assembly. The resultant concentration of cleaved 2-pyridinethione was then measured using UV−vis spectrophotometry against a calibration curve for 2-pyridinethione (λ_{max} = 343 nm).

Fabrication of PMA$_{SH}$ Architectures. Planar PMA$_{SH}$ films were fabricated using a previously described method.[9] For film fabrication on particle templates, a SiO$_2$ (100 μL, 50 g L$^{−1}$) suspension was first washed in ethanol and Milli-Q water, before being dispersed in 100 mM NaOAc buffer (pH 4). Three wash cycles (centrifugation followed by resuspension in 100 μL NaOAc) were performed after the deposition of each polymer layer. For polymer deposition, 50 μL of NaOAc buffer was first added and the washed pellet resuspended via mixing. PMA$_{SH(x)}$ and PVPON polymer solutions (50 μL, 2 mg mL$^{−1}$) were then added, the solution mixed vigorously, and the polymer allowed to adsorb under mild agitation for 15 min. This process was repeated until five PMA$_{SH(x)}$ layers were deposited. The resulting core−shell particles were then oxidized using CaT (2.5 mM) in MES buffer (10 mM, pH 6) for 60 s, resulting in the formation of disulfide cross-links. The particles were suspended in 20 μL of NaOAc, to which 80 μL of HF (5 M, pH 1) was added. *Caution! Hydrofluoric acid is very toxic. Extreme care should be taken when handling HF solution, and only small quantities should be prepared.* The resulting capsules were washed four times via centrifugation (4 min, 4500g) and suspended in 100 μL of NaOAc solution, followed by three centrifugation/wash cycles in 100 μL of PBS solution (10 mM, pH 7.4). The resulting single-component PMA$_{SH}$ HCs were characterized using differential interference contrast (DIC) microscopy (Olympus IX71 microscope, Olympus 100×/1.40 Oil objective) and processed using ImageJ software and algorithms (NIH).[34]

AFM Cantilever Preparation. Both intermittent contact (IC) mode and CP cantilevers were cleaned to remove salt depositions and organics prior to use. The cantilevers were immersed in a 30 vol % 2-propanol solution, followed by Milli-Q water, and then further cleaned using oxygen plasma for 180 s (Harrick Plasma, 0.1 L min$^{−1}$ O$_2$ flow rate, 29.6 W, 300 mTorr). Glass substrates for cantilever spring constant calibration and capsule measurements were cleaned using the same method.

AFM Intermittent Contact Mode Imaging. For IC mode imaging of collapsed HC structures in air, standard tapping mode cantilevers with a spring constant of 40 N m$^{−1}$ (Tap300-G, Budget Sensors, Bulgaria) were used. Images were recorded using a JPK Nanowizard II (JPK Instruments AG, Berlin, Germany). Images were post-treated using accompanying JPK image processing software and algorithms. A three-point first-degree polynomial fit was first subtracted, and then a polynomial fit was subtracted from each scan line independently, excluding capsule regions.

AFM Force Spectroscopy. Force spectroscopy measurements were carried out in PBS (140 mM NaCl, pH 7.4) buffer using a JPK Nanowizard II (The University of Melbourne) for planar film and core−shell particles and a JPK Nanowizard I (Bayreuth University) for HC measurements. Force measurements on planar PMA$_{SH}$ films and CP cantilever calibration and preparation have been described

previously.[9,35] For HC and core−shell particle measurements, PMA_{SH} particles were immobilized onto a PEI-coated glass substrate. The glass substrate was cleaned with 30 vol % 2-propanol and oxygen plasma prior to PEI adsorption. The sample was positioned above an Axiovert 200 microscope (Carl Zeiss MicroImaging, Jena, Germany) with Zeiss objectives (20× and 63× oil). Measurements were conducted by aligning the probe over the center of the visualized colloid, approaching the surface, and then engaging in a "push–pull" cycle with the center axis. This was achieved by lowering the cantilever, until a predetermined force set-point was reached, and then raising the piezo back to its original position. For each measurement, the InvOLS of the PEI-coated glass substrate in working buffer was first determined to allow for accurate postprocessing of the force data. Approach speeds ranging from 0.3 to 1.5 $\mu m\ s^{-1}$ were employed; however, the slopes of the HC force/deformation (F/δ) curves were seen to be independent of approach speed in this range. Each push–pull cycle generated a force-displacement curve for treatment and analysis. Raw AFM data was processed using as-received JPK software to subtract the zero-force baseline during cantilever approach, to set the origin to the initial contact point, and to extract data. The effect of cantilever bending during sample compression was removed using eq 1 to give true sample deformation data

$$\delta = \text{displacement} - (F/k_c) \tag{1}$$

where k_c is the spring constant of the cantilever. For an incompressible material, the force increases with no observable change in deformation, while for softer samples the gradient reduces due to the compliance of the material. Due to possible viscoelastic effects and associated hysteresis, only the approach force curve was analyzed. The stiffness was evaluated to be the linear gradient of the force/deformation curve in the small-deformation regime, corresponding to deformations in the range of the wall thickness (approximately 40 nm), as to negate the effects of capsule permeability.[18] Reported stiffness values are an average of at least 20 measurements on separate capsules, with the error equating to one standard deviation of the data set. For the colloidal probe cantilevers used there was only a small variation in probe radius (16.5 ± 2.0 μm for planar measurements and 15.7 ± 0.2 μm for capsule measurements), and the effect of differences in contact area between samples was discounted. For the $PMA_{SH(20)}$ core−shell particles a probe of radius 16.2 μm was used.

For investigating the force spectroscopy of films and capsules at variable pH, the same experimental methodology was used as previously described. After measurement on the respective systems, ca. 50% of the pH 7.4 buffer was carefully removed via micropipet aspiration to prevent drying, and an equal volume of 100 mM NaOAc buffer (pH 4.0) was gently administered. This was repeated 10 times so that the resulting solution was at pH ∼4.0. The force measurements were then repeated at the new pH value.

Debye−Hückel Screening Length. The screening length (κ^{-1}) was calculated to justify that negligible long-range interactions occur between the colloidal silica probe and the sample. This can be evaluated using eq 2,

$$\kappa^2 = 4\pi\lambda_B n \tag{2}$$

where n is the concentration of monovalent ions and λ_B is the Bjerrum length, which can be approximated as 0.7 nm, the value for water at room temperature. Formally, λ_B can be calculated using eq 3

$$\lambda_B = \frac{e^2}{4\pi\varepsilon_0\varepsilon_r k_B T} \tag{3}$$

where e is the elementary charge, ε_0 the vacuum permittivity, ε_r the relative dielectric constant of the medium, T the absolute temperature of the solution, and k_B Boltzmann's constant. As we use a PBS buffer (140 mM NaCl, $\lambda_B \sim 0.7$ nm), we obtain a value for the Debye−Hückel screening length of approximately 0.9 nm. As the range of indentations used for our measurements and analyses varied between 20 and 100 nm, we can assume that nonzero range interactions in our buffered systems will be negligible. This result aligns with findings in literature for similar experiments.[36]

Applied Probe Axial Strain. As the cantilever probe applies a force to the material, it also exerts an intrinsic axial strain. It is important regarding linear elastic theory that an applied axial strain of 0.2 is not exceeded; otherwise, material nonlinearity becomes an important factor.[19] The axial strain (ε_{zz}) can be evaluated using the active contact radius (a) during compression, where

$$a = \left(\frac{3FR_{eff}(1 - v^2)}{4E_Y}\right)^{1/3} \tag{4}$$

for the Poisson's ratio (v), effective probe radius (R_{eff}), and the Young's modulus (E_Y). This can then be substituted into the equation below, which is developed from the differentiation of the axial displacement field (u_z), where $\varepsilon_{zz} = \delta u_z/\delta z$ and

$$\varepsilon_{zz}(0, 0) = \frac{2a}{\pi R_{eff}(1 - v)} \tag{5}$$

$$u_z(\mathbf{r}, z) = \int\int P_z(r_s)\, G(s)\, dA \tag{6}$$

which can be evaluated according to the approach set out by Landau and Lifshitz. Here P_z is the pressure distribution and $G(s)$ is the Green's function in A, the contact region.[37] We can then model our colloidal probe and capsule system to check the magnitude of the axial strain. When the applied axial strain is modeled for both planar films and capsule systems, it is most sensitive for low Young's modulus and high Poisson's ratio systems. As it is important to only analyze data for applied forces that allow for an axial strain less than 0.2, data collected for both planar and HC samples were only modeled to a maximum force of 1.0 nN. In the case of the low E_Y $PMA_{SH(5)}$ samples, the maximum force studied regarding mechanical properties was 0.7 nN.

RESULTS AND DISCUSSION

PMA−PDA Characterization. The extent of cross-linking between neighboring PMA_{SH} layers is governed by the number of thiol groups that are present in the polymer, which is equivalent to the number of PDA groups per PMA chain (Figure 1). PMA−PDA was synthesized using EDC-activated
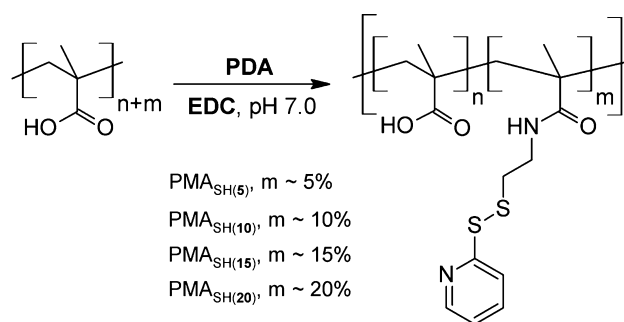
Figure 1. Preparation of PMA−PDA. The extent of pendant PDA modification was quantified using both ${}^1H$ NMR and UV−vis spectrophotometry (m is the target thiol percentage).

amide coupling chemistry.[30] Target mole percentages of PMA−PDA of 5, 10, 15, and 20% were prepared, and the resulting modified polymers are denoted as $PMA_{SH(5)}$, $PMA_{SH(10)}$, $PMA_{SH(15)}$, and $PMA_{SH(20)}$, respectively ($PMA_{SH(x)}$). The extent of PMA functionalization with PDA has been previously determined by comparing the integrals of the aromatic peaks with the peaks from the backbone of PMA−PDA in corresponding ${}^1H$ NMR spectra.[9] The amount of PDA present here was additionally quantified using UV−vis spectrophotometry by measuring the concentration of 2-pyridinethione (343 nm) that is released after reducing the PDA groups with

Scheme 1. Fabrication of Hydrogel Architectures[a]
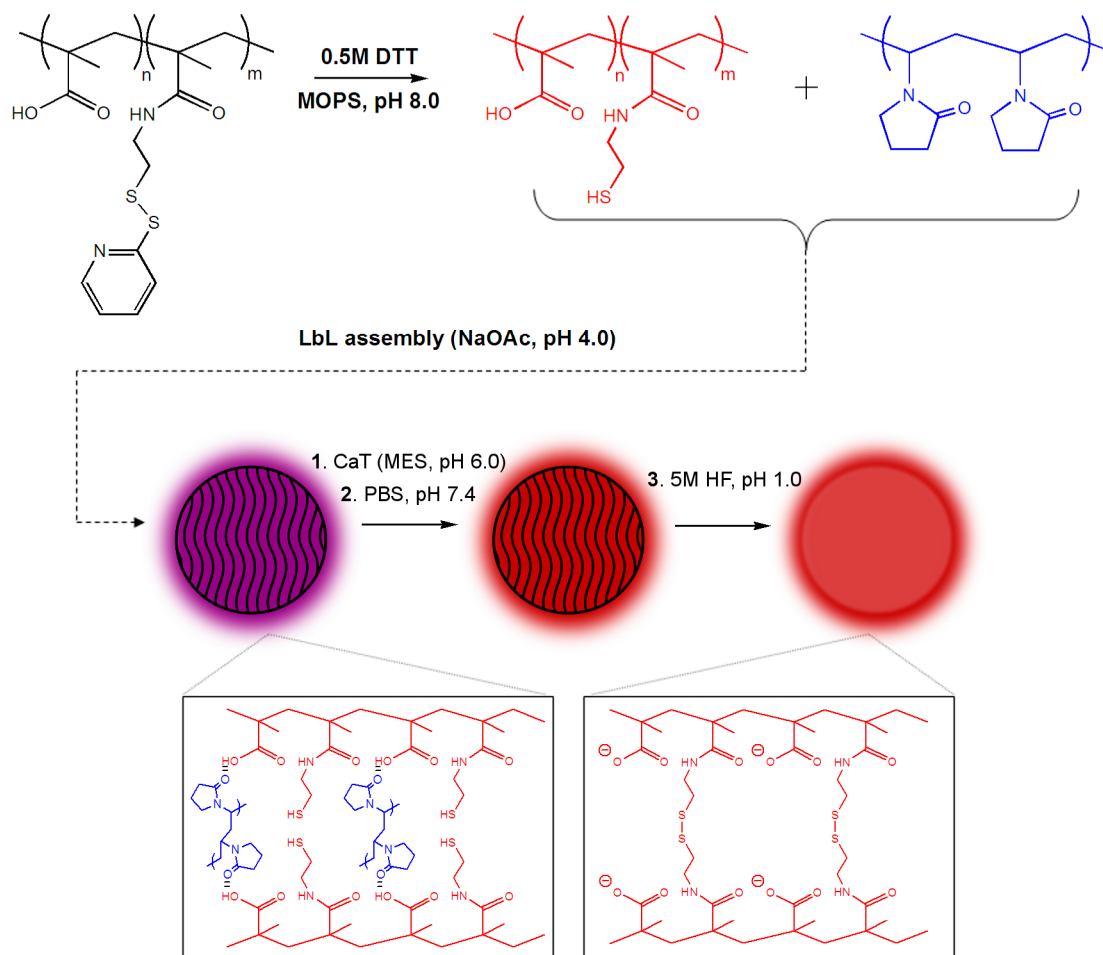
[a]Top: Reduction of PMA−PDA to PMA_{SH(x)} (red). PMA_{SH(x)} and PVPON (blue) are then assembled onto particulate silica templates at pH 4.0 (purple). PMA_{SH(x)} is then oxidized to form stable disulfide cross-links, followed by removal of the PVPON with PBS at pH 7.4. Silica templates were then removed by dissolution using 5 M HF [magnifications show structure before cross-linking (left) and after resuspension in PBS at pH 7.4 (right)]. Five PMA_{SH(x)} layers were deposited.

DTT (pH 8) (Figure S1, Supporting Information). For all measured samples the UV−vis characterization yields lower values by 30−40% of the PMA−PDA modification percentage, when compared to the values that were previously obtained using ^{1}H NMR spectroscopy (Figure S2, Supporting Information). It is likely that the PDA groups of PMA−PDA in aqueous solution are situated in the more hydrophobic regions of the polymer. This diminishes their reactivity and can lead to the mentioned quantification differences, while additionally affecting the actual degree of cross-linking occurring in PMA_{SH} systems. Further, the contribution to the measured differences from small errors in the NMR integration cannot be excluded. However, it is clear from both measurements that there is an increase in PDA substitution with target thiol modification.

Free-Standing PMA_{SH} Capsules. We then investigated the formation of stable, free-standing, hydrogel capsules at physiological pH. PMA_{SH(x)} polymers were used for LbL assembly of films on particle templates (Scheme 1). After the assembly of the planar multilayers, the thiol groups were cross-linked with CaT. Fabrication of free-standing PMA_{SH} capsules was achieved through removal of the silica core using HF, resulting in hollow shells for all modification percentages.

Further washing into PBS solution at pH 7.4 resulted in removal of the PVPON by disrupting the H-bonds, as has been experimentally demonstrated previously,[28] to yield single-component PMA systems. Furthermore, it was observed that all HC systems fabricated were stable over a period of at least 1 week at physiological pH. The resulting swollen capsules were characterized using DIC microscopy in PBS buffer. AFM imaging was used for air-dried capsules immobilized onto a PEI-coated substrate (Figure 2). DIC images in Figure 2 show that with increasing cross-linking degree the optical density of the HCs increases, along with a reduction in the degree of capsule swelling. AFM height image analysis using JPK-SPM data processing software showed that the shell thickness for the dried HCs increased with increasing thiol modification. If we assume that the shell volume is conserved for HC swelling, as proposed by Köhler et al.,[38] then the difference between theoretical shell thickness and measured dry thickness indicates a partial loss of material from the shell wall (Figure 2). Decreasing the number of cross-links leads to less stable hydrogel films, and non-cross-linked material may be lost from the system; this aids capsule expansion at pH 7.4. A general trend was also observed from the AFM scans, where higher cross-linked HCs tended to display more folding features as a
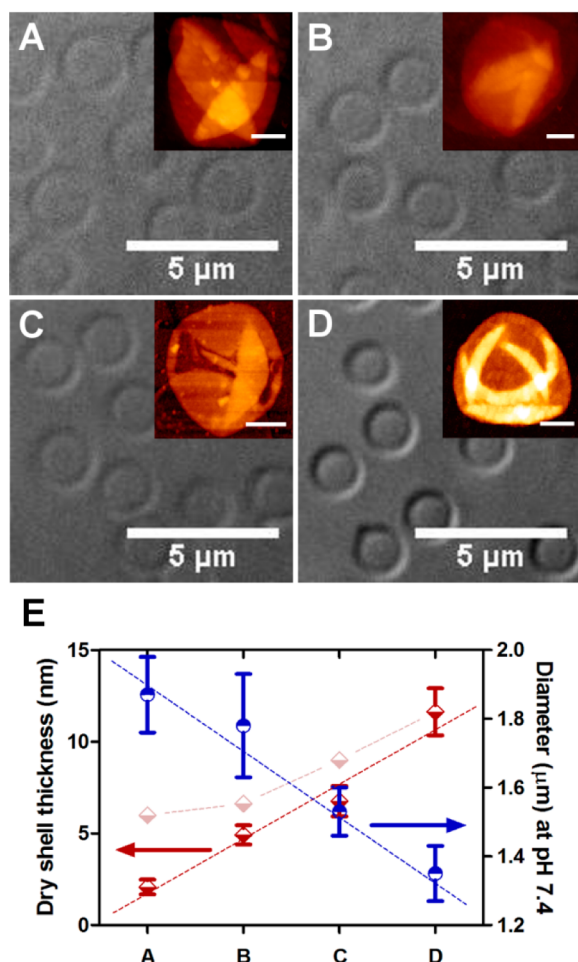
Figure 2. DIC microscopy images of HCs dispersed at pH 7.4. Insets show IC AFM scans of dried HCs immobilized onto a PEI-treated substrate (height range from 0 to 50 nm and scale bar 500 nm, for all images). Images A, B, C, and D represent $PMA_{SH(5)}$, $PMA_{SH(10)}$, $PMA_{SH(15)}$, and $PMA_{SH(20)}$ HCs, respectively. HC diameter at pH 7.4 from DIC microscopy analysis (blue circles), air-dried HC shell thickness (red diamonds) from AFM imaging analysis, and theoretical air-dried shell thickness assuming conservation of shell volume (transparent red diamonds) (E). Error bars represent one standard deviation, and dotted lines are used to guide the eye only.

result of buckling than less-cross-linked HCs. This indicates that higher cross-linked capsules are more rigid.

AFM force spectroscopy measurements were then performed to quantify the mechanical properties of the soft hydrogel materials using CP-AFM and to observe tuning of these properties through variation in cross-linking. In CP-AFM measurements, indentation of hydrogel systems is achieved through controlled piezo movement in the z-direction, with great precision (Figure 3A). As the probe is sensitive to force due to its large surface area, it is important to note that, on the basis of calculations for the Debye−Hückel screening length for the colloidal silica probe in PBS, with 140 mM NaCl, negligible long-range interactions occur between the probe and sample. For all force measurements, there was negligible variation in the radius of the probe used for indentation, and axial strains were kept below 0.2 by analyzing forces <1.0 nN (Figure S3, Supporting Information), allowing us to treat deformations as being linearly elastic. A CP cantilever with a spring constant of 6.8 mN m^{-1} was used for $PMA_{SH(5)}$, while a cantilever with a constant of 66.4 mN m^{-1} was employed for the measurement of all other HCs. It was seen when collecting the AFM force data that approach and retract curves for the $PMA_{SH(10)}$, $PMA_{SH(15)}$, and $PMA_{SH(20)}$ capsule systems all showed considerable hysteresis.

It was previously observed that the deformation of melamine formaldehyde capsules generates hysteresis features, which generally occur for shell-based systems undergoing buckling transitions.[22] The force response for $PMA_{SH(5)}$ HCs was primarily elastic, owing to the extremely soft and compliant nature of the system. Although the stiffer capsules demonstrated a shell-bending behavior, HCs were also compressed multiple times to ca. 50% of their diameter, and it was seen that the force response was unchanged after at least 12 cycles, using a retracted delay time of 1.0 s. This indicates that the HC compressions are elastic to at least 12 deformations and that they retain their original shell conformation after each compression event.

An important requirement for performing force measurements on shells is that the deformation of the shell by the probe is performed uniaxially.[39] This means that the capsule senses the force normal to its center axis. As the diameter of the colloidal bead is approximately 30 times that of the HC, it was expected that the capsule would experience a force similar to a
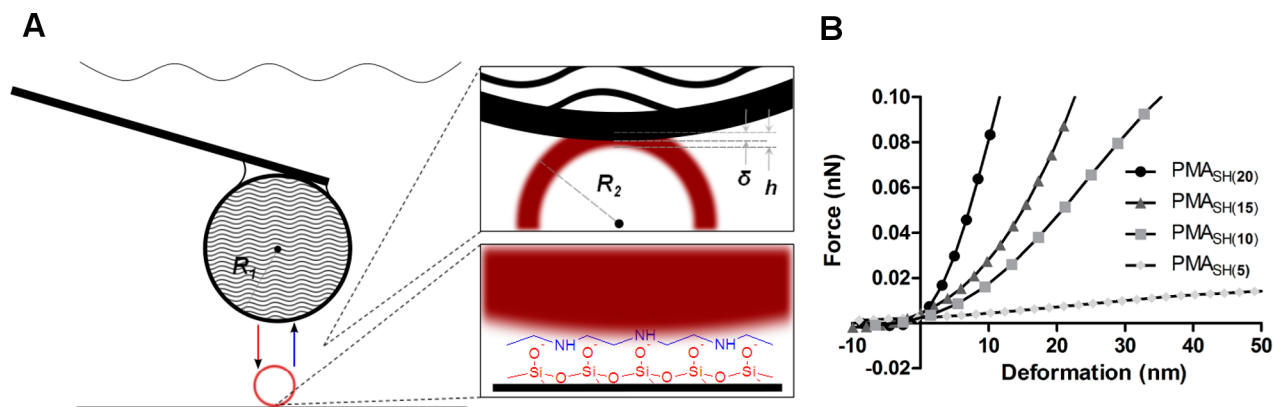
Figure 3. Schematic representation of the CP-AFM technique (A) and representative small-deformation F/δ curves for immobilized HCs (B). An attached glass microsphere (radius R_1) is positioned above an immobilized HC in PBS buffer, from where approach (red arrow) and retract (blue arrow) force curves are generated (A). Top inset depicts deformation (δ) of the HC (shell thickness h, radius R_2) by the CP, while the bottom inset illustrates surface immobilization of the HC using PEI (blue).

parallel plate compression, thereby achieving uniaxial deformation over quite a large radial area. To test this, a 12×12 force map was performed over a $4 \times 4 \ \mu m^2$ area where a single $PMA_{SH(20)}$ HC was immobilized. From Figure S4 (Supporting Information), the force curves collected at points A, B, C, and D give equivalent overall spectra with comparatively equal stiffness values ($14.0 \ mN \ m^{-1}$) over 40 nm of indentation and are constant to 65 nm for spectra A, C, and D. It can therefore be assumed that, due to the relative sizes of the probe and capsule, uniaxial deformation can be achieved over a radius of approximately 2–3 μm.

Analyzing the small-deformation gradient for the HCs (Figure 3B) allowed for determination of the shell stiffness. While the HCs could be tuned between 0.9 and 16.9 mN m^{-1} for 5–20 mol % PDA modification, we previously reported that planar hydrogel films could be tuned between 0.7 and 5.7 mN m^{-1} over the same range.[9] A quadratic increase was observed for the HC structures, whereas the planar film stiffness increased linearly. The basis of this relationship for the HC results can be observed in the Reissner model for thin spherical shells, where the capsule stiffness is proportional to the square of the shell thickness for an isotropic elastic material (eq 7).[40]

$$E_{Y,Reissner} = \frac{FR_{eff}\sqrt{3(1 - v^2)}}{4\delta h^2} \tag{7}$$

This relationship is evident in the data contained in both Figures 2 and 3, where a quadratic relationship must exist between HC stiffness and dry shell thickness, similar to trends observed in the literature.[39] The hydrated shell thickness of low-cross-linked HCs is difficult to quantify accurately. As shown in previous work,[9] low-cross-linked films that experience contraction during dehydration are fragile and lose material. Collapsing a low-cross-linked HC in air and then washing and rehydrating in buffer would result in removal of a portion of the wall material, leading to inaccuracies in determining the wall thickness. In addition, once a capsule collapses, there is increased electrostatic interaction between the PMA_{SH} and surface-bound PEI.

For estimation of the Young's modulus, we assumed that all HCs had an equal hydrated shell volume and that the shell thickness would reduce as the capsules swell with decreasing cross-linking degree. This relationship was demonstrated by Köhler et al. for the thermal shrinking of polyelectrolyte capsules, where it was shown that conservation of the shell volume occurred.[38] We also employed the Reissner relationship for thin shells (eq 7), which has been used previously for modeling the E_Y of polyelectrolyte capsule shells.[41] The applicability of thin shell theory, assumed in the Reissner model, is often limited to a shell thickness to radius ratio of less than 1/20.[42] Collapsed $PMA_{SH(20)}$ HCs have a hydrated shell thickness in PBS buffer of roughly 40 nm (data not shown), with a diameter of 1.35 μm in free suspension. This is equivalent to $h/R \sim 0.06$, greater than the 1/20 limit discussed. Indeed, Mercadé-Prieto et al. utilized finite element modeling to demonstrate that eq 7 only applies to thin shells dependent on bending deformations and that thicker shells require corrections due to considerable Green and Hencky strains.[43]

For E_Y evaluation using the Reissner model, R_{eff} was calculated as a function of both CP and HC radial components. As it was not possible to accurately measure the hydrated shell thickness, h was estimated on the basis of shell volume conservation. More weakly cross-linked HCs expanded at pH

7.4, thereby decreasing the shell thickness, assuming an equal initial mass of polymer adsorbed to the surface for all systems. Using these assumptions, the thickness for the $PMA_{SH(20)}$ system was estimated, and the shell thickness for the other HC systems was based on this. With these values, the Young's modulus of the HCs was found to increase from 0.70 to 2.56 MPa. In the literature, comparable free-standing systems were shown to exhibit elastic moduli typically in the low GPa range.[21] For instance, Glynos et al. found that polylactide microspheres with a cross-linked albumin outer skin had a shell stiffness of 3.8 N m^{-1}, while the E_Y was evaluated to be 2.5 GPa using the Reissner relationship.[15] In contrast, our HCs prove to be remarkably soft and of a similar magnitude to reported collapsed cross-linked PMA capsules evaluated using a Hertz model.[25]

Influence of pH on Film Mechanics. Next, we investigated the potential effect of net shell "pressurization" on the observed enhanced force resistance of the HCs. As this effect would be due to PMA_{SH} charge repulsion in the shell, we studied the swelling behavior and stiffness characteristics of $PMA_{SH(15)}$ capsules at both pH 7.4 and 4.0. As shown in Figure 4, the capsule stiffness increases considerably when the pH is dropped to 4.0. It is postulated that if the shell demonstrated a
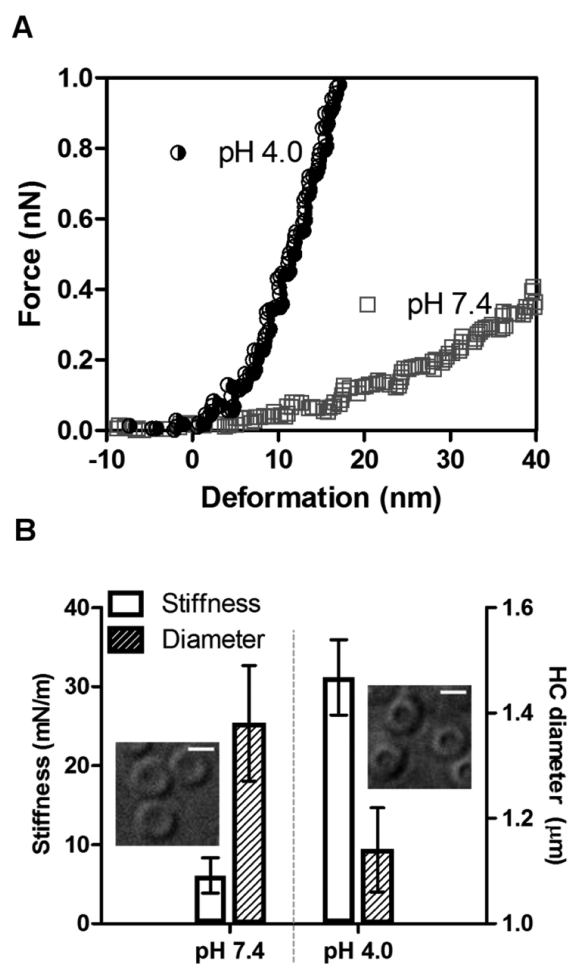

Figure 4. Influence of pH on $PMA_{SH(15)}$ HC stiffness. Representative force curves (A) and DIC microscopy images and stiffness and diameter results (B) for $PMA_{SH(15)}$ capsules at both pH 7.4 and 4.0. Error bars in B correspond to one standard deviation, while scale bars for the DIC images equal 1 μm.

pressurization effect, decreasing the pH and removing the charge repulsion would soften the capsules. As an increase in stiffness is observed with reduced HC swelling, the effect of shell pressurization on force resistance is negligible when compared to other factors.

We then correlated this finding to the pH behavior of PMA_{SH} films fabricated on solid-supported planar structures. $PMA_{SH(20)}$ was used for this experiment as it has previously demonstrated a high degree of stability, so any differences in mechanical properties of the film at different pH values is a function of film behavior rather than possible film disruption during buffer change. Force experiments were performed as per the other PMA_{SH} film measurements;[9] however, after the initial measurement, the pH 7.4 buffer was replaced with buffer at pH 4.0, and the force map was repeated. It was observed that the film thickness decreased to ca. 35 nm and that the stiffness and E_Y both increased roughly 20-fold (Figure 5). We had previously
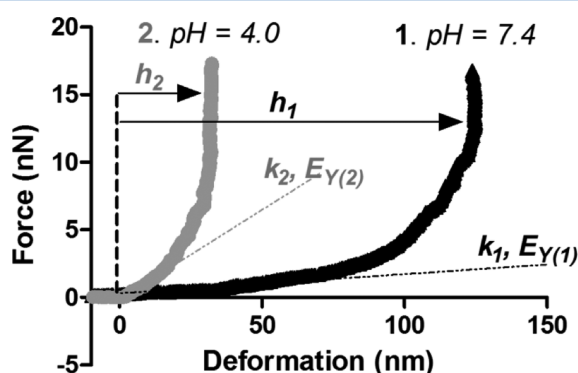

Figure 5. The effect of in situ pH variation on $PMA_{SH(20)}$ film thickness (h) and mechanical properties (k, E_Y) measured using CP-AFM.

observed a general film thickness of 130 ± 50 nm for all $PMA_{SH(x)}$ films,[9] where the film thickness was evaluated as the deformation distance of the probe, from initial contact to substrate incompressibility, on the basis of a literature technique.[44] Sukhishvili and co-workers previously found that EDC-cross-linked PMA films also contracted greatly when the pH was reduced.[24] This can also be related to results published

by Elsner et al. for PMA capsules, where it was found that, as the solution pH decreased below the pK_a of the polymer system, the stiffness increased dramatically due to the formation of hydrogen-bonding interactions.[23] These reports are consistent with our observations that a reduction of the solution pH below the pK_a of PMA_{SH} increases the film density due to the carboxyl group protonation on the polymer backbone.

PMA_{SH} Films Anchored on Particulate Supports. As an intermediate step to the production of free-standing hollow capsules, we examined whether mechanical differences between HCs and planar films may occur due to film formation on particle substrates. The LbL technique was used to adsorb alternating layers of PVPON and $PMA_{SH(20)}$ onto particulate silica templates ($d = 1.11 \ \mu m$) in NaOAc buffer. The hydrogel core−shell particles were cross-linked, dispersed into PBS buffer, and then immobilized onto a PEI-coated glass substrate. Measurements were performed on immobilized colloids visualized optically; the probe was positioned above the center axis of the colloid to achieve uniaxial deformation, and an approach/retract cycle was initiated to measure small material deformations of the film as a function of the applied force. Immobilization is an important aspect of the measurement, as insufficient immobilization can lead to lateral movement during force application and result in poor or misleading spectra. The material stiffness in the small deformation regime was determined from the treated spectra and found to be 2.1 ± 0.4 mN m^{-1}, approximately half that of $PMA_{SH(20)}$ planar films on mica, as shown in Figure 6. This is an interesting observation, as we would expect core−shell particles to be deformed at two contact points when under an applied force: at both the substrate and colloidal probe surfaces. This would lead to a material stiffness half that of the planar hydrogel films, as an incompressible spherical substrate allows for no bending resistance. A further explanation for this was given by Fytas and co-workers when they observed that poly(methyl methacrylate) (PMMA) capsules had different mechanical properties to SiO$_2$−PMMA core−shell particles.[45] Using light-scattering techniques, it was postulated that these differences arose due to differences in the system architecture.

Transition from Planar Films to Hollow Capsules. We previously reported on the mechanical properties of PMA_{SH} planar films on atomically flat mica substrates.[9] It was found
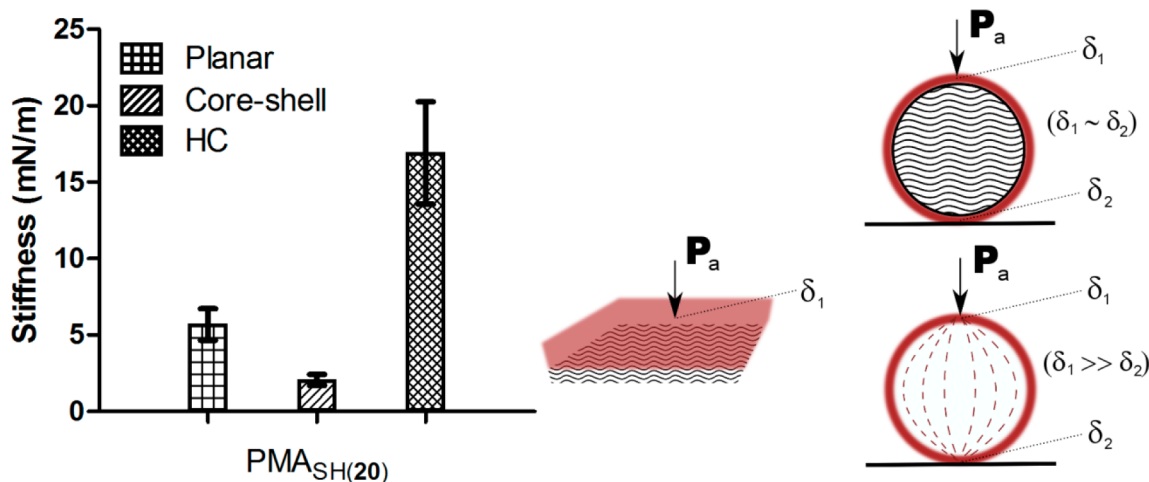

Figure 6. Stiffness values for $PMA_{SH(20)}$ hydrogels confined in planar film, core−shell, and HC architectures. An applied force (P_a) affects a deformation (δ) of the film surface. Error bars represent one standard deviation (planar film data reproduced from ref 9).

that the stiffness of the hydrogel films could be effectively tuned through adjustment of the degree of disulfide-based cross-linking and that all films were mechanically homogeneous over a 50 μm^2 area. From 5 to 20 mol % PDA modification, we reported that the stiffness of the films was found to increase from 0.7 to 5.7 mN m^{-1}, while the E_Y increased from 0.4 to 2.1 kPa using a Hertz model or from 1.0 to 2.3 kPa evaluated using the Johnson−Kendall−Roberts (JKR) model for adhesive contact.[9] All mechanical results were observed to increase linearly with increasing PDA modification. Comparable materials in literature characterized using CP-AFM measurements demonstrate that planar PMA$_{SH}$ films are extremely soft. Using Hertz modeling, soft gelatin films were found to have an E_Y of 20 kPa to 1 MPa,[10] while both the Picart and Singer groups found that, using EDC as a cross-linker, thin hydrogel films could have their modulus tuned between 3 kPa and 1 MPa.[20,46]

In this paper we have shown that the elastic modulus determined for HCs based on Reissner's theory is 3 orders of magnitude greater than those for planar films of the same material. It would generally be assumed that these ranges would be similar, as the material is constant. A possible explanation for these differences was provided by Glynos and co-workers, based on their observation that thick-shelled polymer microspheres had an E_Y approaching that of the bulk material, whereas thinner shelled spheres had a dramatically increased E_Y.[47] They postulated that morphological and molecular restructuring may occur due to confinement in thinner shells and that, as the dimensions approach the nanoscale, surface effects such as surface tension and gradient elasticity can have a profound influence on material properties.[47] In addition, the Reissner model is not directly applicable to the PMA$_{SH}$ HC systems studied. The shell thickness and small diameter of the HCs dictates that they are at, or above, the limit of thin shell theory required for use of the Reissner model. Above this limit, estimates of E_Y are reliant on significant corrections, and accuracy is dependent on accurate shell thickness information.[43] Other assumptions in these models were met, however, as uniaxial deformation and low applied axial strains were achieved during measurement. In addition, this result highlights the requirement of contact mechanics models for soft, viscoelastic, nanostructured hydrogel shells.

The increased HC stiffness observed when compared to planar films fabricated using the same PMA$_{SH(x)}$, as is seen in Figure 7, is of inherent interest. During HC compression, system deformation may occur at the two contact points on the shell surface; however, this will occur predominantly at the CP contact point due to finite energy dissipation through the shell structure via bending resistances. The CP cantilever measures resistance to applied force through both the film and shell bending resistances, if we assume that the HC is not instantaneously permeable to the encapsulated solvent. This would increase the stiffness experienced by the cantilever when compared to the single contact point indentation for films, which allow for increased energy dissipation, as they can be viewed as essentially an infinite plane. Geometrically, spheres have the smallest surface area for a given volume and have a maximized moment of inertia increase around the shell bending axis. This gives a spherical shell structure an increased apparent stiffness when compared to an immobilized membrane of the same material and shell thickness. Further, to our knowledge, planar materials with a system stiffness <5 mN m^{-1} have not been characterized in the literature, and only one example of
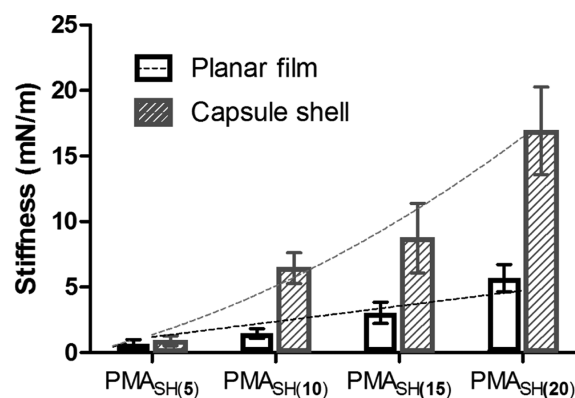
Figure 7. Stiffness comparison results for planar hydrogel films on mica substrates (planar film data reproduced from ref 9) and PEI immobilized HCs. Planar film data are fit with a linear regression, while capsule shell stiffness data are fit with a second-order polynomial. Error bars represent one standard deviation.

similarly soft HCs has been shown,[23] demonstrating the applicability of CP-AFM for this task.

As shown in Figure 7, the planar film stiffness increases linearly with cross-linking degree, as the network becomes increasingly dense and robust to external force. HC stiffness increases at a greater rate with cross-linking, as both the shell becomes more robust and the capsules resist expansion. The increase in stiffness observed for the HCs is a combination of both enhanced material stiffness (shown through increases in film stiffness) and consolidated shell structure (verified based on the observed increases in shell thickness). Previous analyses of PSS/PAH multilayers in planar and capsule configurations demonstrated that capsules tend to have a greater E_Y (1.5−2.0[48] and 1.3−1.9 GPa[14]) when compared to planar films (0.30−0.59 GPa) measured using an elastic buckling technique.[49] Bathe and co-workers were able to show through finite element analysis that the ratio of membrane to bending energies stored within a shell system was highly sensitive to the shell thickness.[50] These results support the argument that the shell structure of PMA$_{SH}$ HCs aids in improving the mechanical stiffness of the system. This finding can be reasoned when considering the bending energies of thin shells and spherical vessels under an applied pressure. On the basis of the Kirchhoff−Love plate theory for elastic shells, the energy change derived from a differential shell geometry is made up of both membrane and bending strains.[51] Due to increased stiffness values for the HCs, we were able to observe these shell resistances for micrometer-sized soft hydrogel capsules when compared to planar films of the same material.

■ CONCLUSIONS

The mechanical properties of PMA$_{SH(x)}$ free-standing hollow capsules with varying degrees of cross-linking were investigated. The stability of these constructs was analyzed using optical and AFM techniques, and it was found that introducing a higher degree of disulfide cross-linking improved both network density and stability. The material compliance was quantified using CP-AFM, and it was found that a hollow capsule architecture offers a greater force resistance when compared to substrate-supported (planar and particulate) films of the same material. It was postulated that this was due to the transfer of the applied force to bending energies within the capsule structure, geometric effects, and shell densification. The mechanical

properties of the PMA_{SH} systems were quantified using the highly sensitive CP-AFM technique, and the results indicated that they were extremely soft and tunable via network density.

We envisage that these results will be useful for researchers involved in the study and characterization of soft and tunable hydrogel shells, in particular for studies where particle material parameters are assumed on the basis of planar film studies. Future work will examine the biological interaction of these materials and the effect that compliance has upon effects such as cellular association and uptake, in vivo clearance rates, cellular adhesion strength, and modulation of biomolecule/conjugate interactions.

■ ASSOCIATED CONTENT

ⓢ Supporting Information

UV−vis spectra for PMA−PDA characterization, applied probe axial strain modeling, and uniaxial deformation AFM force map and spectra for HCs. This material is available free of charge via the Internet at http://pubs.acs.org.

■ AUTHOR INFORMATION

Corresponding Author
*F.C.: e-mail, fcaruso@unimelb.edu.au; tel, +61-3-8344-3461; fax, +61-3-8344-4153. A.F.: e-mail, andreas.fery@uni-bayreuth.de; tel, +49-0-921/55-2753; fax, +49-0-921/55-2059.

Author Contributions
The manuscript was written through contributions of all authors.

Notes
The authors declare no competing financial interest.

■ ACKNOWLEDGMENTS

■ ABBREVIATIONS

AFM, atomic force microscopy; CaT, N-chloro-p-toluenesulfonamide sodium salt; CP, colloidal probe; DIC, differential interference contrast; DTT, dithiothreitol; EDC, 1-ethyl-3-(3-dimethylaminopropyl)carbodiimide; HC, hydrogel capsule; HF, hydrofluoric acid; IC, intermittent contact; InvOLS, inverse optical lever sensitivity; JKR, Johnson−Kendall−Roberts; LbL, layer-by-layer; MES, 2-(N-morpholino)-ethanesulfonic acid; MOPS, 3-(N-morpholino)propanesulfonic acid; MWCO, molecular weight cutoff; NaOAc, sodium acetate; NMR, nuclear magnetic resonance; PBS, phosphate-buffered saline; PDA, 2-(2-pyridinyldithio)ethaneamine; PEI, polyethyleneimine; PMA, poly(methacrylic acid); PMA-Na, poly(methacrylic acid, sodium salt); PMA_{SH}, thiol-modified poly(methacrylic acid); PMMA, poly(methyl methacrylate); ppm, parts per million; PVPON, poly(N-vinylpyrrolidone); QCM-D, quartz crystal microgravimetry; UV−vis, ultraviolet−visible.

■ REFERENCES

(1) Hoare, T. R.; Kohane, D. S. Hydrogels in Drug Delivery: Progress and Challenges. *Polymer* **2008**, *49*, 1993−2007.

(2) Becker, A. L.; Johnston, A. P. R.; Caruso, F. Layer-by-Layer-Assembled Capsules and Films for Therapeutic Delivery. *Small* **2010**, *6*, 1836−1852.

(3) Nguyen, K. T.; Shukla, K. P.; Moctezuma, M.; Braden, A. R. C.; Zhou, J.; Hu, Z.; Tang, L. Studies of the Cellular Uptake of Hydrogel Nanospheres and Microspheres by Phagocytes, Vascular Endothelial Cells, and Smooth Muscle Cells. *J. Biomed. Mater. Res. Part A* **2009**, *88A*, 1020−1030.

(4) Stuart, M. A. C.; Huck, W. T.; Genzer, J.; Müller, M.; Ober, C.; Stamm, M.; Sukhorukov, G. B.; Szleifer, I.; Tsukruk, V. V.; Urban, M. Emerging Applications of Stimuli-Responsive Polymer Materials. *Nat. Mater.* **2010**, *9*, 101−113.

(5) Best, J. P.; Yan, Y.; Caruso, F. The Role of Particle Geometry and Mechanics in the Biological Domain. *Adv. Healthcare Mater.* **2012**, *1*, 35−47.

(6) Yan, Y.; Such, G. K.; Johnston, A. P. R.; Best, J. P.; Caruso, F. Engineering Particles for Therapeutic Delivery: Prospects and Challenges. *ACS Nano* **2012**, *6*, 3663−3669.

(7) Banquy, X.; Suarez, F.; Argaw, A.; Rabanel, J.-M.; Grutter, P.; Bouchard, J.-F.; Hildgen, P.; Giasson, S. Effect of Mechanical Properties of Hydrogel Nanoparticles on Macrophage Cell Uptake. *Soft Matter* **2009**, *5*, 3984−3991.

(8) Georges, P. C.; Janmey, P. A. Cell Type-Specific Response to Growth on Soft Materials. *J. Appl. Physiol.* **2005**, *98*, 1547−1553.

(9) Best, J. P.; Javed, S.; Richardson, J. J.; Cho, K. L.; Kamphuis, M. M. J.; Caruso, F. Stiffness-Mediated Adhesion of Cervical Cancer Cells to Soft Hydrogel Films. *Soft Matter* **2013**, *9*, 4580−4584.

(10) Domke, J.; Radmacher, M. Measuring the Elastic Properties of Thin Polymer Films with the Atomic Force Microscope. *Langmuir* **1998**, *14*, 3320−3325.

(11) Kovalev, A.; Shulha, H.; Lemieux, M.; Myshkin, N.; Tsukruk, V. Nanomechanical Probing of Layered Nanoscale Polymer Films with Atomic Force Microscopy. *J. Mater. Res.* **2004**, *19*, 716−728.

(12) Markutsya, S.; Jiang, C.; Pikus, Y.; Tsukruk, V. V. Freely Suspended Layer-by-Layer Nanomembranes: Testing Micromechanical Properties. *Adv. Funct. Mater.* **2005**, *15*, 771−780.

(13) Schmidt, S.; Zeiser, M.; Hellweg, T.; Duschl, C.; Fery, A.; Möhwald, H. Adhesion and Mechanical Properties of PNIPAM Microgel Films and Their Potential Use as Switchable Cell Culture Substrates. *Adv. Funct. Mater.* **2010**, *20*, 3235−3243.

(14) Dubreuil, F.; Elsner, N.; Fery, A. Elastic Properties of Polyelectrolyte Capsules Studied by Atomic-Force Microscopy and RICM. *Eur. Phys. J. E* **2003**, *12*, 215−221.

(15) Glynos, E.; Sboros, V.; Koutsos, V. Polymeric Thin Shells: Measurement of Elastic Properties at the Nanometer Scale Using Atomic Force Microscopy. *Mater. Sci. Eng., B* **2009**, *165*, 231−234.

(16) Ye, C.; Drachuk, I.; Calabrese, R.; Dai, H.; Kaplan, D. L.; Tsukruk, V. V. Permeability and Micromechanical Properties of Silk Ionomer Microcapsules. *Langmuir* **2012**, *28*, 12235−12244.

(17) Ducker, W. A.; Senden, T. J.; Pashley, R. M. Direct Measurement of Colloidal Forces Using an Atomic Force Microscope. *Nature* **1991**, *353*, 239−241.

(18) Fery, A.; Dubreuil, F.; Möhwald, H. Mechanics of Artificial Microcapsules. *New J. Phys.* **2004**, *6*, 18−30.

(19) Dimitriadis, E. K.; Horkay, F.; Maresca, J.; Kachar, B.; Chadwick, R. S. Determination of Elastic Moduli of Thin Layers of Soft Material Using the Atomic Force Microscope. *Biophys. J.* **2002**, *82*, 2798−2810.

(20) Francius, G.; Hemmerle, J.; Ohayon, J.; Schaaf, P.; Voegel, J. C.; Picart, C.; Senger, B. Effect of Crosslinking on the Elasticity of Polyelectrolyte Multilayer Films Measured by Colloidal Probe AFM. *Microsc. Res. Tech.* **2006**, *69*, 84−92.

(21) Pretzl, M.; Neubauer, M.; Tekaat, M.; Kunert, C.; Kuttner, C.; Leon, G. r.; Berthier, D.; Erni, P.; Ouali, L.; Fery, A. Formation and Mechanical Characterization of Aminoplast Core/Shell Microcapsules. *ACS Appl. Mater. Interfaces* **2012**, *4*, 2940−2948.

(22) Lulevich, V. V.; Andrienko, D.; Vinogradova, O. I. Elasticity of Polyelectrolyte Multilayer Microcapsules. *J. Chem. Phys.* **2004**, *120*, 3822−3826.

(23) Elsner, N.; Kozlovskaya, V.; Sukhishvili, S. A.; Fery, A. pH-Triggered Softening of Crosslinked Hydrogen-Bonded Capsules. *Soft Matter* **2006**, *2*, 966−972.

(24) Kozlovskaya, V.; Kharlampieva, E.; Mansfield, M. L.; Sukhishvili, S. A. Poly(methacrylic acid) Hydrogel Films and Capsules: Response to pH and Ionic Strength, and Encapsulation of Macromolecules. *Chem. Mater.* **2006**, *18*, 328–336.

(25) Drachuk, I.; Shchepelina, O.; Lisunova, M.; Harbaugh, S.; Kelley-Loughnane, N.; Stone, M.; Tsukruk, V. V. pH-Responsive Layer-by-Layer Nanoshells for Direct Regulation of Cell Activity. *ACS Nano* **2012**, *6*, 4266–4278.

(26) Becker, A. L.; Zelikin, A. N.; Johnston, A. P. R.; Caruso, F. Tuning the Formation and Degradation of Layer-by-Layer Assembled Polymer Hydrogel Microcapsules. *Langmuir* **2009**, *25*, 14079–14085.

(27) Chong, S. F.; Lee, J. H.; Zelikin, A. N.; Caruso, F. Tuning the Permeability of Polymer Hydrogel Capsules: An Investigation of Cross-Linking Density, Membrane Thickness, and Cross-Linkers. *Langmuir* **2011**, *27*, 1724–1730.

(28) Zelikin, A. N.; Li, Q.; Caruso, F. Disulfide-Stabilized Poly(methacrylic acid) Capsules: Formation, Cross-Linking, and Degradation Behavior. *Chem. Mater.* **2008**, *20*, 2655–2661.

(29) Saito, G.; Swanson, J. A.; Lee, K.-D. Drug Delivery Strategy Utilizing Conjugation via Reversible Disulfide Linkages: Role and Site of Cellular Reducing Activities. *Adv. Drug Delivery Rev.* **2003**, *55*, 199–215.

(30) Zelikin, A. N.; Quinn, J. F.; Caruso, F. Disulfide Cross-Linked Polymer Capsules: En Route to Biodeconstructible Systems. *Biomacromolecules* **2005**, *7*, 27–30.

(31) Shimoni, O.; Postma, A.; Yan, Y.; Scott, A. M.; Heath, J. K.; Nice, E. C.; Zelikin, A. N.; Caruso, F. Macromolecule Functionalization of Disulfide-Bonded Polymer Hydrogel Capsules and Cancer Cell Targeting. *ACS Nano* **2012**, *6*, 1463–1472.

(32) Zelikin, A. N.; Li, Q.; Caruso, F. Degradable Polyelectrolyte Capsules Filled with Oligonucleotide Sequences. *Angew. Chem., Int. Ed.* **2006**, *45*, 7743–7745.

(33) Zelikin, A. N.; Becker, A. L.; Johnston, A. P. R.; Wark, K. L.; Turatti, F.; Caruso, F. A General Approach for DNA Encapsulation in Degradable Polymer Microcapsules. *ACS Nano* **2007**, *1*, 63–69.

(34) Abramoff, M. D.; Magelhaes, P. J.; Ram, S. J. Image Processing with ImageJ. *Biophotonics Int.* **2004**, *11*, 36–42.

(35) Attard, P. Measurement and Interpretation of Elastic and Viscoelastic Properties with the Atomic Force Microscope. *J. Phys.: Condens. Matter* **2007**, *19*, 473201–473233.

(36) Francius, G.; Hemmerlé, J.; Ohayon, J.; Schaaf, P.; Voegel, J.-C.; Picart, C.; Senger, B. Effect of Crosslinking on the Elasticity of Polyelectrolyte Multilayer Films Measured by Colloidal Probe AFM. *Microsc. Res. Tech.* **2006**, *69*, 84–92.

(37) Landau, L. D.; Lifshitz, E. M. *Theory of Elasticity*; Pergamon Press Ltd: Oxford, 1959; pp 30–36.

(38) Köhler, K.; Shchukin, D. G.; Möhwald, H.; Sukhorukov, G. B. Thermal Behavior of Polyelectrolyte Multilayer Microcapsules. 1. The Effect of Odd and Even Layer Number. *J. Phys. Chem. B* **2005**, *109*, 18250–18259.

(39) Elsner, N.; Dubreuil, F.; Weinkamer, R.; Wasicek, M.; Fischer, F. D.; Fery, A. Mechanical Properties of Freestanding Polyelectrolyte Capsules: A Quantitative Approach Based on Shell Theory Characterization of Polymer Surfaces and Thin Films. *Prog. Colloid Polym. Sci.* **2006**, *132*, 117–123.

(40) Reissner, E. Stresses and Small Displacements of Shallow Spherical Shells. *J. Math. Phys.* **1946**, *25*, 80–85.

(41) Fery, A.; Weinkamer, R. Mechanical Properties of Micro- and Nanocapsules: Single-Capsule Measurements. *Polymer* **2007**, *48*, 7221–7235.

(42) Gregory, R. D.; Milac, T. I.; Wan, F. Y. M. A Thick Hollow Sphere Compressed by Equal and Opposite Concentrated Axial Loads: An Asymptotic Solution. *SIAM J. Appl. Math.* **1998**, *59*, 1080–1097.

(43) Mercadé-Prieto, R.; Thomas, C. R.; Zhang, Z. Mechanical Double Layer Model for *Saccharomyces Cerevisiae* Cell Wall. *Eur. Biophys. J.* **2013**, DOI: 10.1007/s00249-013-0909-x.

(44) McNamee, C. E.; Yamamoto, S.; Higashitani, K. Preparation and Characterization of Pure and Mixed Monolayers of Poly(ethylene Glycol) Brushes Chemically Adsorbed to Silica Surfaces. *Langmuir* **2007**, *23*, 4389–4399.

(45) Still, T.; Sainidou, R.; Retsch, M.; Jonas, U.; Spahn, P.; Hellmann, G. P.; Fytas, G. The "Music" of Core–Shell Spheres and Hollow Capsules: Influence of the Architecture on the Mechanical Properties at the Nanoscale. *Nano Lett.* **2008**, *8*, 3194–3199.

(46) Boudou, T.; Crouzier, T.; Auzely-Velty, R.; Glinel, K.; Picart, C. Internal Composition versus the Mechanical Properties of Polyelectrolyte Multilayer Films: The Influence of Chemical Cross-Linking. *Langmuir* **2009**, *25*, 13809–13819.

(47) Glynos, E.; Koutsos, V.; McDicken, W. N.; Moran, C. M.; Pye, S. D.; Ross, J. A.; Sboros, V. Nanomechanics of Biocompatible Hollow Thin-Shell Polymer Microspheres. *Langmuir* **2009**, *25*, 7514–7522.

(48) Gao, C.; Donath, E.; Moya, S.; Dudnik, V.; Möhwald, H. Elasticity of Hollow Polyelectrolyte Capsules Prepared by the Layer-by-Layer Technique. *Eur. Phys. J. E* **2001**, *5*, 21–27.

(49) Nolte, A. J.; Rubner, M. F.; Cohen, R. E. Determining the Young's Modulus of Polyelectrolyte Multilayer Films via Stress-Induced Mechanical Buckling Instabilities. *Macromolecules* **2005**, *38*, 5367–5370.

(50) Bathe, K.-J.; Chapelle, D.; Lee, P.-S. A Shell Problem 'Highly Sensitive' to Thickness Changes. *Int. J. Numer. Meth. Eng.* **2003**, *57*, 1039–1052.

(51) Love, A. E. H. The Small Free Vibrations and Deformation of a Thin Elastic Shell. *Philos. Trans. R. Soc. A* **1888**, *179*, 491–546.